Experimental study on a modified Savonius wind rotor for street lighting systems. Analysis of external appendages and elements

Experimental study on a modified Savonius wind rotor for street lighting systems. Analysis of external appendages and elements.

S. Montelpare, R. Ricci, V. D'Alessandro, A. Zoppi

Experimental study on a modified Savonius wind rotor for street lighting systems. Analysis of external appendages and elements.☆

Sergio Montelpare[b,*], Valerio D'Alessandro[a], Andrea Zoppi[a], Renato Ricci[a]

[a] *Marche Polytechnic University, Industrial Engineering and Mathematical Sciences Department (DIISM)*
Via Brecce Bianche 1, 60131 Ancona (Italy)
[b] *University "G. d'Annunzio" of Chieti-Pescara, Engineering and Geology Department (INGEO)*
Viale Pindaro 42, 65127 Pescara (Italy)

Abstract

This paper is aimed at investigating the performance of a Savonius generator in the presence of external aerodynamic appendages. The Savonius generator is a slender (high aspect ratio) vertical axis wind turbine and is part of a public lighting system (a street lamp) powered by renewable energy sources, particularly wind and solar energy. The external elements are self aligning systems, a conveyor and a deflector, used to increase the rotor's aerodynamic performance. The high aspect ratio, required for architectural integration, and the use of self aligning aerodynamic appendages distance this Savonius assembly from all the other ones tested in previous research works. For this reason, new tests have been carried out in static and dynamic conditions on a

☆This document is a collaborative effort.

*Corresponding Author
Email addresses: s.montelpare@unich.it (Sergio Montelpare), v.dalessandro@univpm.it (Valerio D'Alessandro), a.zoppi@univpm.it (Andrea Zoppi), ricci@univpm.it (Renato Ricci)

1:1 scale model in the Environmental Wind Tunnel (EWT) of Marche Polytechnic University (UNIVPM); three different rotors at different wind velocities were analyzed for each possible combination of aerodynamic appendages. The results showed that the rotor's performance could be increased with the simultaneous application of a conveyor and deflector, reaching a maximum power coefficient of about 0.3. Also static measurements were performed on a locked rotor at different angles of attack. The torque angular distribution showed a periodic behavior with no negative torque values.
Keywords: VAWT, experimental measurements, wind tunnel, Savonius rotor, wind energy, street lamp, external appendages, renewable energies

1. Introduction

The Savonius rotor is a vertical axis rotor of simple geometry and in its most common shape it is composed of two semi-cylindrical blades, asymmetrically positioned with respect to the vertical axis of rotation. It is named after the Finnish engineer S.J. Savonius, the owner of its first patent, which dates back to 1930s [1, 2]. The principle mechanism of this machine is extremely simple. Motion is generated by the torque as a consequence of the drag imbalance between the advancing bucket, which is hit by the flow on its concave side, and the returning bucket which moves in the opposite direction of the air flow. Since the point where the resultant of these two forces works is not located along the rotational axis of the rotor, an aerodynamic moment is generated, which makes the system rotate. A well designed Savonius turbine can reach tip speed ratios (λ) higher than 1.00, reaching rotational speeds higher than the velocity of the incident wind, which indicates that

the rotor has also a lift behavior. Speaking in terms of power coefficient C_P, defined as the relationship between the power extracted and the power of the air flow diverted, studies have found values of C_P in the range of 0.15 and 0.25. Despite these values being very low when compared with those of other types of wind turbines [3, 4], the Savonius rotor has come back into interest, since:

- it is very simple and economic;
- it works in any wind direction;
- it has a high static torque, therefore it starts easily;
- it requires little maintenance;
- it is not noisy;
- it is compact;
- it can be easily integrated into vertical structures.

Hence, this kind of generator is particularly suitable for low power applications in urban environments, characterized by highly turbulent flows that vary considerably in direction.

For these reasons, a Savonius rotor with a high aspect ratio was chosen as wind generator by the Marche Polytechnic University (UNIVPM) in a project dealing with an urban system powered by renewable sources [5]. Such system consists in a street lamp, powered by solar and wind energy (Fig. 1), to be used in urban environments; each renewable source is connected to a controllable DC/DC converter and their outputs are stored in a lead acid battery bank. The lamppost may be used in a network or standalone configuration. The solar energy is supplied by a 200 $[W]$ photovoltaic panel placed on the upper end of the lamppost, while three wind generators are inserted along

the support structure. The innovative idea at the base of the architectural design was precisely the insertion of the Savonius rotors inside the lamppost structure, since commercial solutions typically provide a wind generator on the top. In order to place the rotor inside a slender structure authors used a high aspect ratio and the aerodynamic performance of the basic rotor assembly, which are not available in literature for this stretched configuration, were analyzed in a previous work [6].

In addition external appendages were designed to increase the Savonius performance and the purpose of the present study was to examine their combined effect with a high aspect ratio rotor. These structures, conversely to different ones analyzed by other authors, are aerodynamically profiled to increase the turbine power coefficient and particularly to be self aligning with the wind direction: they consist in a Conveyor and a Deflector. The experimental tests were carried out in the Environmental Wind Tunnel (EWT) of UNI-VPM in dynamic and static conditions on 1:1 scale models. The results are illustrated in terms of $C_P - \lambda$ and $C_{TS} - \theta$ plots, where C_{TS} is the static torque coefficient and θ is the angular position.

2. Brief overview of Savonius literature

Throughout the years many authors have studied this wind rotor, obtaining maximum power coefficients in the range of 0.10 - 0.25 and focusing their attention on a low aspect ratio, which resulted in the best choice. Several review articles have tried to summarize the many numerical and experimental works carried out [7, 8]. It is worth pointing out that our choice to design slender rotors with a high aspect ratio, that is not "the best choice", derives

from restrictions due to the architectural integration inside the street lamp; besides there are not literature studies that optimize this configuration.

Many researches have been carried out on the role of the parameters defining the geometry of the rotor, the main of which are illustrated in Fig. 2. In some cases the authors of these studies reached contrasting conclusions. The presence of an open overlap, for example, was positively evaluated by many authors [9–13], who agreed in suggesting an optimum overlap ratio between 10 and 15%. In these conditions it is possible to observe some overlap flows that increase the pressure on the concave side of the returning bucket, thus reducing the overall drag [14–16]. At the same time, other authors evaluated the presence of overlap negatively when applied to slightly modified geometries [17, 18]. There is general agreement in literature on the periodic behavior of the torque angular distribution, with periodicity equal to the number of rotor blades [18–20]. Analyses carried out on a revolution of the static torque highlighted high mean values, which make the starting of the rotor easier, but were connected to wide oscillations. These oscillations generate minimum torque values, which can be also negative since they can give starting problems at certain wind angles and most of all cause unpleasant cyclic stress to the structures [21]. Such problems can be overcome by employing rotors with a higher number of blades and staggered stages [21–25], or alternatively by using blades that are twisted along their vertical axis. Even in this case there are different opinions in literature: according to some [26, 27] the twist or the addition of stages increases the maximum C_P of the rotor, contrary to the results obtained by others [19, 28]. Many of these contrasting conclusions are due to the extreme complexity of the motion field

[10, 14, 29–31] combined with the system's low performance levels: slight geometric variations or inaccuracies in the experimental set-ups can considerably affect the performance obtained. An example is given in [6], where the effects produced on the experimental set-up when the bearings are changed are illustrated.

Such disagreements have encouraged authors of this paper to analyze the effect of the external appendages on rotors with different twist and an open overlap.

A shared opinion is that a way to increase the rotor's low performance levels can be to use external appendages. In most cases these appendages can be classified in shields (also called deflectors) and conveyors. Deflectors are used to protect the returning blade from the incident flow. In [32] a dihedral screen placed upstream the turbine is investigated. In this case the portion of fluid that would have ended on the returning blade is diverted towards the advancing one. By doing so the fluid dynamic characteristics in which the rotor works are modified, even though the amount of fluid is the same. The result is an improvement in the performance levels with an increase of +19.7% for C_P and of 2.3 times for λ_{max}. In [33] the numerical analyses carried out by applying a deflector on a Savonius rotor show a $C_{P,max}$ of 0.25 (vs 0.17 of the traditional rotor). Conveyors are used to redirect a greater portion of fluid towards the rotor and are often employed together with deflectors. In [34–36] the experimental and numerical analyses of a particular combination of Deflector and Conveyor in the optimal configuration show variations of $C_{P,max}$ and of λ_{max} from 0.15 to 0.38 and from 0.67 to 0.9, respectively. The increase in performance is considerable, however it is nec-

essary to point out that in the calculation of the C_P values only the cross section of the rotor was taken into account, which, when appendages are used, can be smaller than the actual cross section of the fluid diverted. This means that in these conditions the increase in the power extracted from the fluid can be influenced by the greater amount of fluid processed. In [37] the Conveyor and the Deflector are integrated in a "Guide-Box Tunnel (GBT)" with adjustable inlet and exit sections, reaching a $C_{P,max}$ equal to $\lambda = 0.27$ and a λ_{max} of 1.8 in the optimal configuration. In this case the GBT does not cause an increase but rather a decrease in the actual cross section of the fluid diverted.

3. Experimental apparatus

3.1. The Environmental Wind Tunnel (EWT)

The EWT is a closed circuit wind gallery as shown in Fig. 3. Its test chamber has three main test sections: the first section is used for aerodynamic tests, like the ones described in this paper, requiring a uniform velocity distribution and a low turbulence level. The second is used to test reciprocal interference effects between slender bodies. The third one is the environmental section and is used to test wind effects over buildings, structures and orography models that are subjected to fully developed environmental boundary layers. The wind tunnel is equipped with a fan having a constant rotational speed of 975 $[RPM]$ and 16 blades with an adjustable pitch. The test section cross sectional area is 3.16 $[m^2]$ and the inlet wind speed ranges between 6 $[m/s]$ and 40 $[m/s]$. Measurements with Constant Temperature Hot Wire Anemometer (CTA HWA) showed a deviation from the average

speed lower than 2.5% and a turbulence intensity lower than 0.3% over more than 90% of the test cross section. A compact heat exchanger is used to control temperature fluctuations within a range of 1 [$^{\circ}C$] around the ambient.

3.2. The rotor models

The rotors studied in this work are Savonius rotors with semi-circular blades in 1:1 scale with respect to those designed for the street lamp, whose geometric characteristics are illustrated in Fig. 2. For this kind of rotor most authors (such as [9, 12, 21, 38]) agree on an optimal configuration, whose characteristics are shown in Table 1. Several of these parameters, except aspect ratio, were adopted for the Savonius rotor tested in this paper, while others were modified in order to facilitate the lamppost industrial production, improve structural stiffness and favor integration inside the street lamp structure Fig. 1. The models without aerodynamic appendages have a frontal area of 0.384 [m^2], while it increases to 0.828 [m^2] in presence of conveyor and deflector . The blockage factor, introduced by [39] and defined in eq. (1) is respectively 3.04% and 6.55%. Considering also the frontal area of the support structure (frame), the total blockage reaches a maximum of 7.78%. When calculating the incoming wind speed, a correction procedure was applied to take into account the blockage effect according to eq. (2) introduced in [39].

$$\epsilon = \frac{A_t}{4S} \tag{1}$$

$$v = v_{\infty}(1+\epsilon) \tag{2}$$

The rotor is composed of modular elements axially connected along a central shaft with a $d = 37$ $[mm]$ diameter. Such elements can be aligned or staggered by a certain angle with respect to the vertical axis. In this way it is possible to give the rotor a straight or a twisted geometry (helical rotor). In this work three rotors were analyzed (Fig. 4): two helical rotors with steps of 90° and 105° and a straight rotor (0°). The helical step corresponds to the relative rotation angle between the two end sections. The maximum step of 105° is a construction requirement of the firms in charge of building the end products. The vertical surfaces of the blades are made of a polyethylene sheet that can follow the double curvature given by the twist. The sheet is fixed to the modular ribs and stretched so as to have a solid and regular surface for the flow. Near the rotational axis there is gap a of 18 $[mm]$ for the flow to pass through. Referring to Fig. 2, the geometric characteristics of the rotors tested are summarized in Table 2.

3.3. Aerodynamic appendages

The aerodynamic appendages external to the rotor are coverings used to optimize performance by acting on the incident flow. This system is composed of a Deflector and a Conveyor. The Conveyor is used to direct a greater portion of fluid towards the advancing blade, increasing the frontal section of incidence. Moreover, the built Conveyor also extends to the rear part of the rotor so as to increase the angular excursion of the area where conveyed flow interacts with the advancing blade. The Deflector, instead, is used to reduce the resistant torque by shielding the returning blade. The working positions of the two elements is schematized in 5. The two elements are integral with one another and they are both hooked to runners fixed on

the rotor's supporting disks. Travelling along the runners under the action of the torques generated when they are hit by the air flow, they move to the position of minimum resistance to the wind. In this way they self-align with the wind and the Savonius rotor can continue to work in every incident wind direction.

4. The measurements setup and procedure

Depending on the wind speed, an operation point is identified when the system reaches a constant average rotational speed. In this point the average values of the driving forces (from fluid dynamics actions) and the resistant forces (friction, loads) are equal. The main load in wind generators is the electric generator connected to the rotor with the task of transforming the rotational mechanical energy into electrical energy. In the tests performed, this load was generated with a mechanical disk brake by modulating the pressure on the caliper; in this way it is possible to apply different loads. The measurement procedure can be briefly summarized:

- The desired incoming wind velocity is settled by adjusting the wind tunnel rotor blades pitch.
- The disk brake is opened to ensure a no load condition and to leave the rotor free to run at its maximum rational speed.
- The disk caliper is displaced by an endless screw to obtain fine tuning and to slow the Savonius rotor down to a desired RPM.
- Once a stable condition is achieved, angular velocity and load cell output are acquired.

- the last two points are repeated until a blocked rotor configuration is attained.

By measuring the torque T and the angular velocity ω, according to eq. eq. (3)-(4), the tip speed ratio λ and the torque and power coefficients C_T and C_P were obtained.

$$C_T = \frac{T}{\frac{1}{2}\,\rho\,A\,R\,v^2} \qquad \lambda = \frac{R\,\omega}{v} \tag{3}$$

$$C_P = \frac{P}{\frac{1}{2}\,\rho\,A\,v^3} = \lambda\,C_T \tag{4}$$

The definitions given follow literature and consider the cross section of the rotor (A), even though it does not always coincide with that of the diverted flow. Indeed, with the use of appendages the frontal section of the system can sometimes increase or decrease, causing the cross section of the diverted flow and consequently also the processed flow to vary. The angular velocity ω is obtained by an incremental encoder ELTRA EL40 having a resolution of 14400 ppr. A radial lever arm, integrated with the braking system, transmits the torque T on a mono-axial load cell fixed to the frame. The load cell was calibrated before the tests, using sample weights. The load cell is a DS Europe 546QD having a measuring range of $0 \div 60[kg]$, a maximum error lesser than $\pm 0.046\% FS$ and a sensitivity of $2[mV/V]FS$ typical. The torque is obtained from the simple relationship $T = Fl$, where F is the force measured on the load cell and l the length of the lever arm. The apparatus here described is illustrated in Fig. 6. Tests were performed at different free stream velocities and a real time National Instrument DAQ system had collected measurements with an acquisition period of 3 $[s]$ and a sampling frequency of 1024 $[Hz]$.

5. Evaluation of measurement uncertainties

Torque and angular velocity are characterized by various factors of uncertainty, that were classified as type A or type B. Type A are associated with random fluctuations that occur during acquisitions: the uncertainties related to the mean values obtained for each measurement point, given a population standard deviation σ and N acquired values, were calculated by eq. (5).

$$\sigma_{ave} = \frac{\sigma}{\sqrt{N}} \tag{5}$$

Type B uncertainties are related to calibration and accuracy of the sensors, so they were directly derived from technical specifications of the instrument used; i.e. the load balance. Since neither of the two types of errors include the other, the overall uncertainty was obtained according to eq. (6).

$$\sigma = \sqrt{\sigma_A^2 + \sigma_B^2} \tag{6}$$

Regarding the derived quantities, such as torque and power coefficients, the error propagation law (7) was used.

$$f = f(x, y) \quad \Longrightarrow \quad \sigma_f = \sqrt{\left(\frac{\partial f}{\partial x}\sigma_x\right)^2 + \left(\frac{\partial f}{\partial y}\sigma_y\right)^2} \tag{7}$$

All the graphs of the experimental results are plotted with error bars corresponding to a confidence level of 95%, which reflects an interval of $\pm 2\sigma$. In addition, all the maximum C_p values are reported in tables with the same confidence level.

6. Experimental Results

Several configurations were investigated and they are all summarized in Tab. 9, where the respective reference codes and the main results are illustrated. Each configuration was tested in dynamic conditions at different wind velocities v_∞, ranging from 7 to 12 $[m/s]$. From the tests carried out the curves of T, P vs ω, as well as those of the coefficients C_T and C_P vs λ, were obtained according to data described in Sec. 4. The points in the diagram refer to the experimental values, while the fitting curves are third order polynomials optimized by the least squares method. To simplify the reading of the diagrams it is best to choose one of the tests as a reference. In our case, we chose the test performed with the standard Savonius rotor [6], that is a two straight bladed rotor with end plates and internal gap. We opted for this combination because it is the most common in literature. The performance obtained with this test are shown in Fig. 7. Fig. 7a and 7b illustrate the performance observed at different wind velocities in absolute terms, while Fig. 7c and Fig. 7d show the relative curves of C_P/C_T vs λ. These latter curves can be taken as reference for the rotor's performance because they do not depend on the velocity of the incident flow (they are independent of the Reynolds number). The fact that in some cases the curves of the different velocities do not perfectly coincide is due to the mechanical frictions of the test system. Further details can be found in [6]. To make the comparison between the different performances easier, we drew an horizontal line corresponding to the maximum C_P of the reference test, which is equal to 0.245, in the plots illustrating the curves of $C_P - \lambda$.

6.1. Effect of the Conveyor

A conveyor is an appendage that increases the frontal surface of the system. It works by directing a portion of the fluid that otherwise would flow outside the rotor towards the advancing blade. As a result, an increase in performance is expected due to the larger amount of fluid processed by the rotor. The tested conveyor extends downstream to the rear part of the rotor, so as to increase the interaction between the conveyed flow and the advancing blade. Fig. 8 illustrates the results obtained for the rotors without appendages and for those with the Conveyor, which are indicated with the white and the black circles respectively. The results show a performance improvement, in terms of $C_{P,max}$, of some percentage points and the straight rotor showed a lower increment with respect to the helical rotors. Therefore it can be deduced that the conveyor used has a positive effect for all the tested configurations. In Tab. 3 the improvements obtained are illustrated in numerical terms.

6.2. Effect of the Deflector

A deflector is an appendage that shields part of the frontal surface of the rotor. In particular, it stops the air flow from directly hitting the returning blade, that is the blade returning towards the wind direction. The aim is clearly to reduce the overpressure on the returning blade and therefore the drag torque. The deflector built for our tests has a "tail", whose aim is to contribute together with the Conveyor to the alignment of the appendages to the wind. The effect obtained with the application of the Deflector is shown in Fig. 8c, where the white and gray circles respectively indicate the rotors without appendages and those with the Deflector. The rotor with a step of

105°(Fig. 8c) was tested without end plates. From the tests carried out a drop in performance, both in terms of $C_{P,max}$ and λ_{max}, can be observed. The drop is greater for the rotors with a step of 0° and 90°. The causes of this drop in performance can be found in the possible stagnation pressure between the blade and the internal surface of the deflector, and in the lower amount of diverted fluid. The former acts as resistance to rotation of the blade, the latter is due to the fact that the Deflector deflects the flow towards the outside of the rotor (see Fig. 5). 2D numerical analyses [29] supported these hypotheses. Tab. 4 illustrates the results obtained in numerical terms.

6.2.1. Joint effect of the Conveyor and the Deflector

The effect of the simultaneous presence of the Conveyor and the Deflector is illustrated in the plots in Fig. 9, where the black and the white circles respectively indicate the tests with and without the appendages. Results show that, unlike the situation with the Deflector only, there is no performance drop. However, the simultaneous presence of both the appendages produce different effects in the three rotors. In the case of the straight rotor (Fig. 9a) there is considerable increase in $C_{P,max}$ while the maximum tip speed ratio (λ_{max}) remains unaltered. In the case of the helical rotor with a step of 90° (Fig. 9b) the increase in $C_{P,max}$ is limited, similarly to the results obtained with the Conveyor only (see Fig. 8b). In this particular case it is possible to observe a shift of the curve to the left (black circles), towards lower values of the tip speed ratio for both $C_{P,max}$ and λ_{max}. In the case of the helical rotor with a step of 105° and without end plates (Fig. 9c, white and black circles) a similar behavior to that of the straight rotor can be observed, with an increase in C_P while λ remains the same. With the employment of end plates

(Fig. 9c gray and white triangles) the behavior observed is different: there is no improvement in $C_{P,max}$, which actually slightly decreases. Furthermore the same shift of the curve towards the left, i.e. towards lower values of λ, can be observed also in the case of the rotor with a step of 90°. Tab. 5 shows the variations of $C_{P,max}$ obtained in the tests described above.

6.3. Effect of the posts on the appendages

One of the technical solutions taken into consideration in the street lamp project is to use support posts that serve as a frame for the structure. They are steel tubular poles with a diameter of 42 $[mm]$. The posts are positioned externally at a distance of 635 $[mm]$ between the center of the rotor and the vertical axis of the posts. In the most unfavorable layout shown in Fig. 5 the posts are placed at angular intervals of 90°. From previous studies [6] it emerged that the posts negatively affect the rotor's performance for two reasons: a) for the leeward wake that disturbs the flow incident to the rotor; b) for the overpressure generated on the blade approaching the posts.

The negative effect exerted on the rotors with no aerodynamic appendages can reach - 31.4% of $C_{P,max}$, although it is not the same for all the rotors: the helical rotor with a step of 105° is less affected (-17.9%). The effect of the posts was tested employing the Conveyor and the Deflector used both singularly and in combination. Fig. 10 illustrates the effects on the $C_P - \lambda$ curves of the simultaneous presence of the posts and the Conveyor. Fig. 10a refers to the straight rotor, Fig. 10b to the helical rotor with a step of 90°. In the graphs the dotted curve marked with *"x"* represents the performance of the rotor with no posts and no appendage (which is taken as a reference). The black circles represent the performance of the rotor with the appendage (in

this case the Conveyor). The white circles represent the results obtained with the simultaneous employment of the posts and the aerodynamic appendage. The same symbols were used for the results obtained with the simultaneous application of the posts and the Deflector (Fig. 11) and that of the posts, the Conveyor and the Deflector (Fig. 12). The variations in performance in terms of $C_{P;max}$ are illustrated in Tab. 6. From the results obtained it is possible to see that C_P decreases considerably with the employment of the posts and the Conveyor, while the respective tip speed ratios decrease less appreciably (Fig. 10). In practice, the curves drop and shift slightly to the left. This means that the performance severely diminishes due to the presence of the posts, which cause disturbance to the flow incident on the rotor.

When adding the posts to the rotor equipped with the Deflector the behavior of the rotor changes radically (Fig. 11). In this case the presence of the posts has actually a positive effect, since the performance increase in terms of both C_P and λ. We previously saw that the presence of the Deflector was highly detrimental, probably due to the overpressure between the blade and the internal part of the Deflector. The blade moving upward would have to face this overpressure for the whole route covered by the Deflector: practically a sector of about 90°. It is possible that in the presence of the posts the overpressure on the returning blade is reduced to two very limited areas, which are the areas occupied by the posts. Hence the relative improvement in performance, which however is still lower than that obtained with the rotor without the posts and without the Deflector. When the posts are applied to the rotor equipped with both the Conveyor and the Deflector the performance decreases once again, as it can be seen in Fig. 12. In terms of

C_P, the decrease is different depending on the type of rotor: for the straight rotor, in fact (Fig. 12a) the decrease is more pronounced, while for the helical rotor with a step of 90° it is less conspicuous (Fig. 12b). In terms of λ no significant variations can be observed. Even in the presence of the posts, the best configuration is the one with both the Conveyor and the Deflector. This is, in fact, the less penalizing configuration, given that the performance remains very close to that of the rotors of reference without posts and without appendages.

6.4. Effect of the twist on the appendages

The effect produced by the twist on the rotor's performance was already studied in [6], where the authors showed that the different helical steps have little effect on the $C_P - \lambda$ curves. Compared to the straight rotor, the rotor with a step of 90° exhibited a slight decrease in $C_{P,max}$, between 6% and 7.4% for the cases with and without the end plates respectively. The behavior of the rotor with a step of 105°, instead, was very similar to that of the straight rotor. In Fig. 13 the results obtained with the three rotors for the different combinations of appendages are compared. The white circles refer to the straight rotor, the black ones to the rotor with a step of 90° and the gray triangles to the rotor with a step of 105°. All the rotors are equipped with end plates. With the employment of the Conveyor only (Fig. 13a) it is worth noting that the effect of the twist is negligible and all the rotors have very similar performance. A different behavior is observed only when the Deflector is applied, as shown in Fig. 13b. In this case the drop in C_P as previously described mainly affects the straight rotor and the one with a step of 90°. The rotor with a step of 105°, while having a considerable decrease

in performance, proves to produce better results than the other two rotors. Finally, in the case where both the Conveyor and the Deflector are applied (Fig. 13c) the performance improvement in terms of C_P mainly affects the straight rotor, while the twisted ones continue to have similar performance to that observed in the case of the Conveyor only (Fig. 13a). The results of the tests described above are shown in Tab. 7.

6.5. Static Tests

The static tests were performed by blocking the rotor with the disk caliper at different angular positions, that were measured as the angle between the chord of the blade and the direction of the incident wind (Fig. 2). The angle was measured in the lower end section of the rotor. The measurements were performed on a complete revolution with a step of 10° and the main results are reported in Tab. 8. The effects of the helical step on the static torque for the rotors with end plates and aerodynamic appendages are shown in Fig. 14. It can be observed that the twist has the ability to strongly reduce the amplitude of the sinusoid (up to 40%). Also the static torque average value is reduced by 10-13%. This causes a more regular distribution of the angular torque and therefore less cyclic stress on the structure. The absence of negative values for the torque in the tests illustrated indicates the possibility of the rotors to self-start in every wind direction. The angular position of the peaks of C_{TS} of the helical rotors are relative, as they depend on the reference section chosen and on the rotors' height. Fig. 15 illustrates the static torque plots of the helical rotor with a step of 105° with and without the external appendages (conveyor and deflector). The plot of the rotor with the external appendages has bigger average and amplitude values (up of

32%). This mean that also in static conditions these appendages modify the flow-rotor interactions creating this bigger torque. In Fig. 16 the effects of the posts on the rotor with aerodynamic appendages and no helical step are shown. The two plots are almost the same: this indicates that the posts have minimal effect on the flow that reaches the rotor. So the performance loss detected in dynamic conditions could be mainly due to the interaction between the posts and the rotating blades.

7. Concluding remarks

This paper presents the results of experimental investigations carried out on a high aspect ratio Savonius rotor with three different helical steps: 0°, 90°and 105°. These rotors are part of a street lamp powered by renewable energy currently under study at UNIVPM. The tests were performed in a closed circuit wind tunnel to evaluate the effects of the application of single or combined self aligning aerodynamic appendages on the rotor's performance. The main findings of this study are here summarized:

- The use of a rotor twist, in absence of external appendages, does not significantly modify the obtainable maximum power coefficient and the main advantages are related to the more stable torque in the rotor revolution.
- The use of a deflector placed very close to the rotor induces very poor performance for every tested configuration and this is due to the counteracting overpressure that occurs in the narrow channel between the deflector and the returning blade. This phenomenon was also observed in a numerical work previously published [29]. The use of a rotor twist

slightly reduces the negative effect of the deflector due to the non-simultaneous effects on the vertical rotor axis.

- The use of a conveyor, that increases the processed air flow, induces positive effects especially for the straight rotor. In the author's opinion this is due to the fact that both conveyor and rotor should have the same twist.
- The simultaneous presence of a straight deflector and conveyor gives the best performance in the case of the rotor with no twist, which underlines the need to design these appendages with a strong relation to the rotor twist.
- The presence of support posts placed externally to the rotor blades gives a negative effect with poor measured performance. This is due to the flow separations that exhibit the posts on the conveyor side and to the overpressure induced on the returning blades for the deflector side. The use of external appendages reduces this phenomenon, but a negative effect concerning cases without posts remains.

In conclusion, the use of external appendages is recommended if a combined configuration is selected. The use of straight appendages should be coupled with a rotor having a 0° twist and to preserve the positive effect of a twist rotor designers should employ stacked and staggered straight rotors. The presence of two profiled conveyors and deflectors allows for a self aligning system that is able to modify its orientation with respect to the incoming wind direction without the use of an external moving apparatus.

8. Acknowledgments

This work was realized thanks to the support of the projects IPA P.O.W.E.R.E.D and the Ministry of Economic Development INDUSTRIA 2015 (www.powered-ipa.it).

9. References

[1] S. J. Savonius, The S-rotor and its applications, Mechanical Engineering 5 (53) (1931) 333–338.

[2] S. J. Savonius, The wing rotor in theory and practice, Savonius Co., 1928.

[3] R. E. Wilson, P. B. Lissaman, Applied Aerodynamics of wind power machines, no. GI-41840 in Research Applied to National Needs, Oregon State University, 1974.

[4] A. Jha, Wind Turbine Technology, ISBN 13: 978-1-4398-1507-6, CRC Press, 2011.

[5] R. Ricci, D. Vitali, S. Montelpare, An innovative wind–solar hybrid street light: development and early testing of a prototype, International Journal of Low-Carbon Technologies 10 (4) (2015) 420–429.

[6] R. Ricci, R. Romagnoli, S. Montelpare, D. Vitali, Experimental study on a Savonius wind rotor for street lighting systems, Applied Energy 161 (2016) 143–152.

[7] J. V. Akwa, H. A. Vielmo, A. P. Petry, A review on the performance of Savonius wind turbines, Renewable and Sustainable Energy Reviews 16 (5) (2012) 3054 – 3064, ISSN 1364-0321.

[8] S. Roy, U. K. Saha, Review on the numerical investigations into the design and development of Savonius wind rotors, Renewable and Sustainable Energy Reviews (23) (2013) 73–83.

[9] N. Fujisawa, On the torque mechanism of Savonius rotors, Journal of Wind Engineering and Industrial Aerodynamics 40 (1992) 277–292.

[10] N. Fujisawa, F. Gotoh, Visualization study of the flow in and around a Savonius rotor, Experiments in Fluids (12) (1992) 407–412.

[11] N. Fujisawa, Velocity measurements and numerical calculations of flow fields in and around Savonius rotors, Journal Of Wind Engineering And Industrial Aerodynamics 59 (1996) 39–50.

[12] B. F. Blackwell, R. E. Sheldahl, L. V. Feltz, Wind tunnel performance data for two and three bucket Savonius rotors, United States Energy Research and Development Administration under contract AT .

[13] R. Ricci, S. Montelpare, G. Borrelli, V. D'Alessandro, Experimental Analysis of a Savonius Wind Rotor for Streetlighting Systems, in: Thermal and Environmental issue in energy systems, Sorrento, Italy, 603–607, 2010.

[14] V. D'Alessandro, S. Montelpare, R. Ricci, A. Secchiaroli, Unsteady Aerodynamics of a Savonius wind rotor: a new computational approach

for the simulation of energy performance, Energy 35 (8) (2010) 3349–3363.

[15] R. Ricci, S. Montelpare, A. Secchiaroli, V. D'Alessandro, Flow field assessment in a vertical axis wind turbine, WIT Transactions on Engineering Sciences 69 (2010) 255–266.

[16] Z. Driss, O. Mlayeh, S. Driss, D. Driss, M. Maaloul, M. S. Abid, Study of the bucket design effect on the turbulent flow around unconventional Savonius wind rotors, Energy 89 (2015) 708 – 729.

[17] V. J. Modi, M. S. U. K. Fernando, On the performance of the Savonius wind turbine, Journal of Solar Energy Engineering 111 (1989) 71–81.

[18] M. A. Kamoji, S. B. Kedare, S. V. Prabhu, Experimental investigations on single stage modified Savonius rotor, Applied Energy 86 (7-8) (2009) 1064–1073.

[19] M. Kamoji, S. Kedare, S. Prabhu, Performance tests on helical Savonius rotors, Renewable Energy 34 (3) (2009) 521–529.

[20] S. Frikha, Z. Driss, E. Ayadi, Z. Masmoudi, M. S. Abid, Numerical and experimental characterization of multi-stage Savonius rotors, Energy 114 (2016) 382 – 404, ISSN 0360-5442.

[21] T. Hayashi, Y. LI, Y. Hara, Wind tunnel tests on a different phase three-stage Savonius rotor, JSME International Journal 48 (1, series B).

[22] J. L. Menet, A double-step Savonius rotor for local production of electricity: a design study, Renewable Energy 29 (11) (2004) 1843–1862.

[23] N. Mahmoud, El-Haroun, E. Wahba, M. Nasef, An experimental study on improvement of Savonius rotor performance, Alexandria Engineering Journal (51) (2012) 19–25.

[24] J. Kumbernuss, J. Chen, H. Yang, L. Lu, Investigation into the relationship of the overlap ratio and shift angle of double stage three bladed vertical axis wind turbine (VAWT), Journal of Wind Engineering and Industrial Aerodynamics (107-108) (2012) 57–75.

[25] B. A. Bhayo, H. H. Al-Kayiem, Experimental characterization and comparison of performance parameters of S-rotors for standalone wind power system, Energy 138 (2017) 752 – 763.

[26] U. K. Saha, M. Rajkumar, On the performance analysis of Savonius rotor with twisted blades, Renewable Energy 31 (11) (2006) 1776–1788.

[27] U. K. Saha, S. Thotla, D. Maity, Optimum design configuration of Savonius rotor through wind tunnel experiments, Journal of Wind Engineering and Industrial Aerodynamics 96 (8-9) (2008) 1359–1375.

[28] K. Golecha, T. Eldho, S. Prabhu, Influence of the deflector plate on the performance of modified Savonius water turbine, Applied Energy (88) (2011) 3207–3217.

[29] M. Tartuferi, V. D'Alessandro, S. Montelpare, R. Ricci, Enhancement of savonius wind rotor aerodynamic performance: A computational study of new blade shapes and curtain systems, Energy 79 (C) (2015) 371–384.

[30] I. Dobrev, F. Massouh, CFD and PIV investigation of unsteady flow through Savonius wind turbine, Energy Procedia (2011) 711–720.

[31] A. Shigetomi, Y. Murai, Y. Tasaka, Y. Takeda, Interactive flow field around two Savonius turbines, Renewable Energy (2011) 536–545.

[32] B. M. Shaughnessy, S. D. Probert, Partially-blocked savonius rotor, Applied Energy (43) (1992) 239–249.

[33] M. Mohamed, G. Janiga, E. Pap, D. Thevenin, Optimization of Savonius turbines using an obstacle shielding the returning blade, Renewable Energy 35 (11) (2010) 2618–2626.

[34] B. Altan, M. Atilgan, An experimental and numerical study on the improvement of the performance of Savonius wind rotor, Energy Conversion and Management 49 (12) (2008) 3425–3432.

[35] B. D. Altan, M. Atilgan, A. Özdamar, An experimental study on improvement of a Savonius rotor performance with curtaining, Experimental Thermal and Fluid Science 32 (2008) 1673–1678.

[36] B. Altan, M. Atilgan, The use of a curtain design to increase the performance level of a Savonius wind rotors, Renewable Energy 35 (4) (2010) 821–829.

[37] K. Irabu, J. N. Roy, Characteristics of wind power on Savonius rotor using a guide-box tunnel, Experimental Thermal and Fluid Science 32 (2007) 580–586.

[38] M. Nakajima, S. Iio, T. Ikeda, Performance of double-step Savonius rotor for environmentally friendly hydraulic turbine, Journal of Fluid Science and Technology 3 (3) (2008) 410–419.

[39] A. Pope, J. B. Barlow, W. H. Rae, Low-Speed Wind Tunnel Testing, John Wiley & Sons, 3rd edn., 1999.

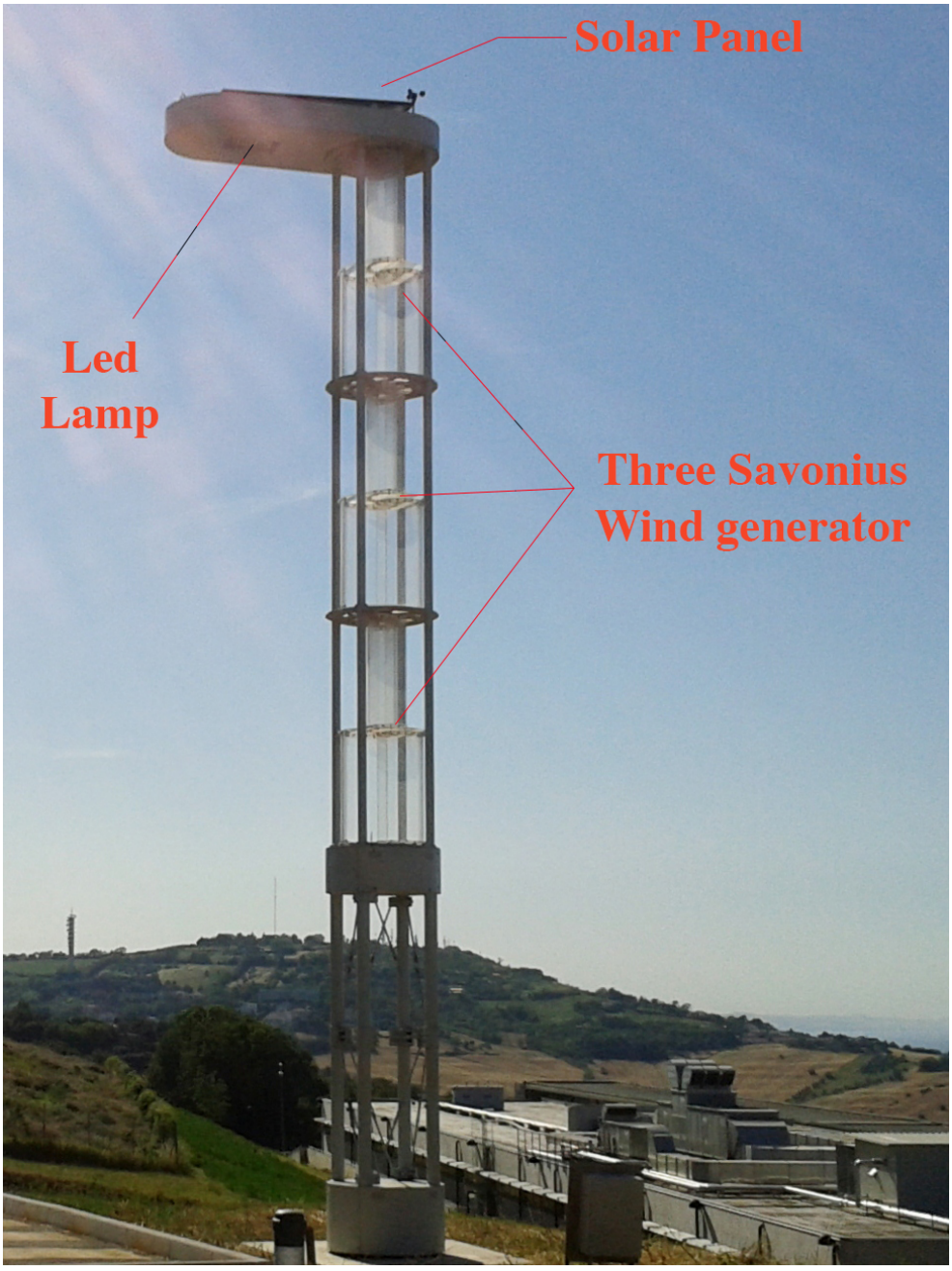

Fig. 1: The prototype of the experimental street lamp powered by renewable energy sources.

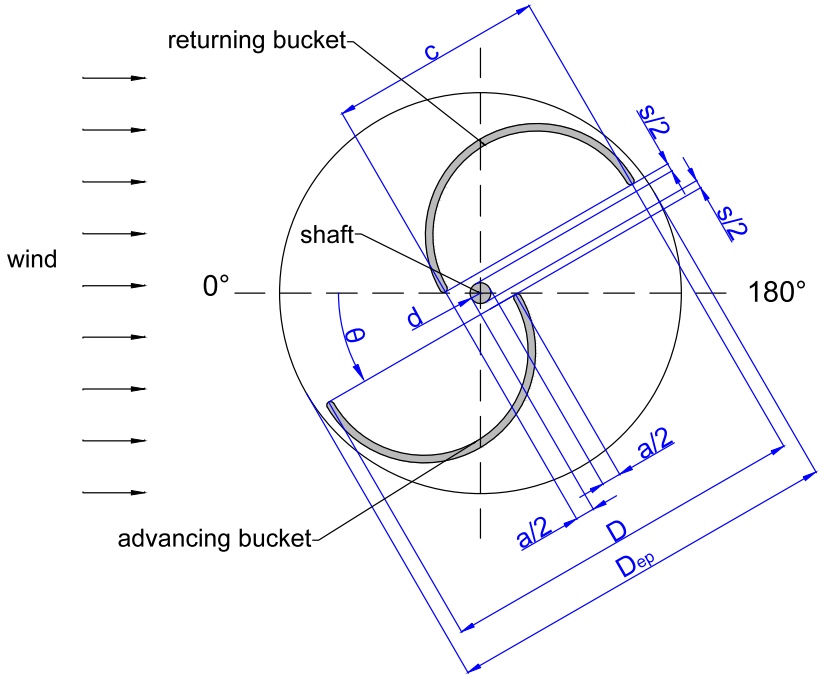

Fig. 2: Schematic representation of a classic Savonius rotor section.

Fig. 3: The Environmental Wind Tunnel of the Marche Polytechnic University

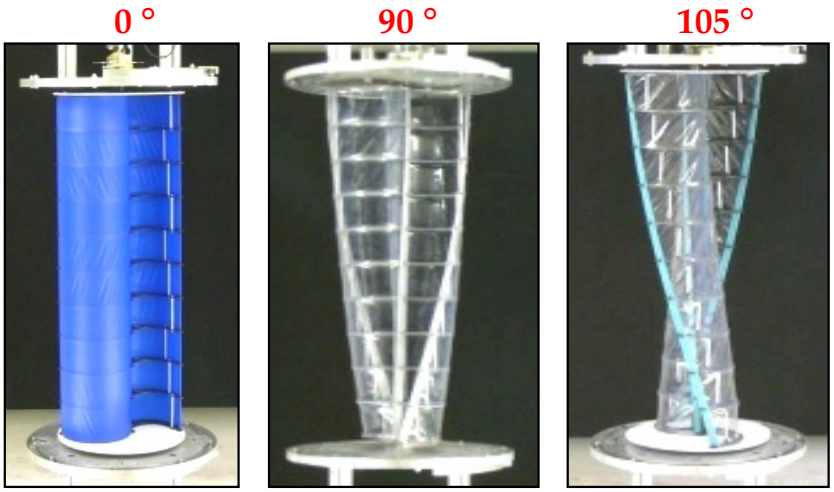

Fig. 4: The rotors tested in the present work

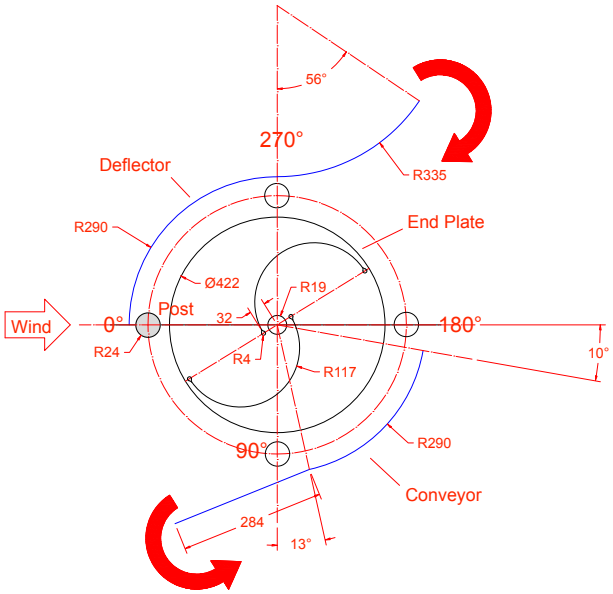

Fig. 5: Diagram of the elements surrounding the rotor in the tests performed.

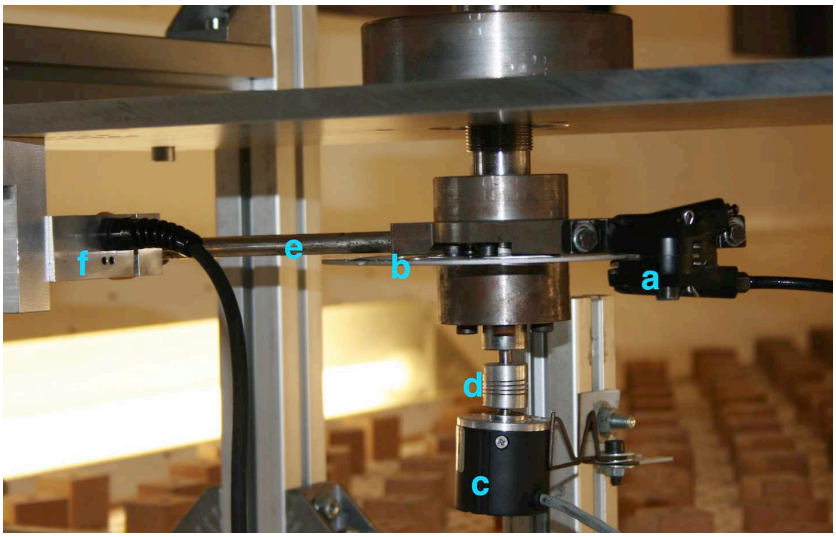

Fig. 6: Details of the experimental apparatus: a) brake caliper b) break disk c) encoder d) joint e) lever arm f) load cell

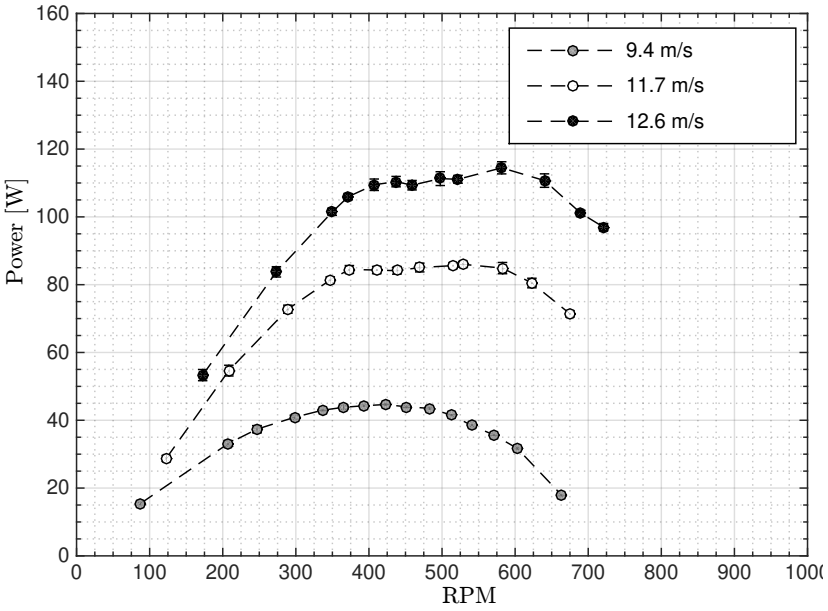

(a) Power

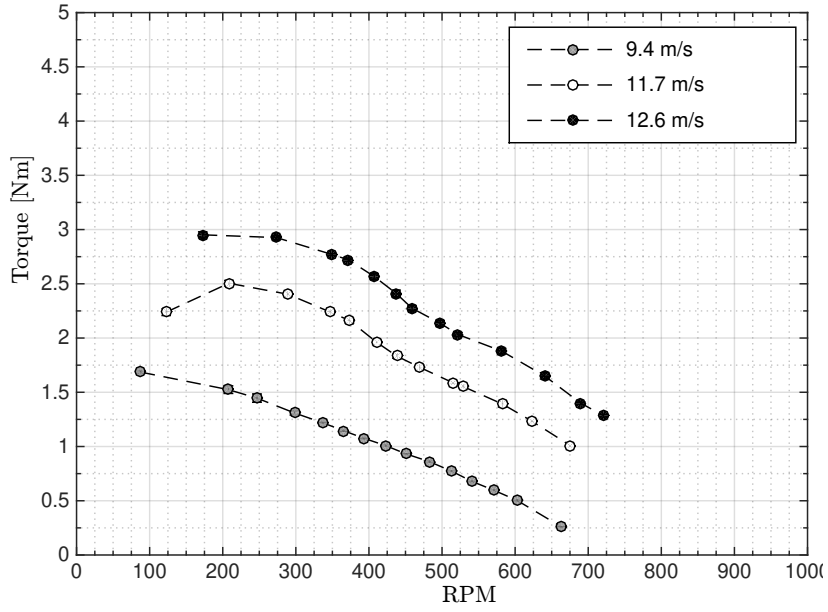

(b) Torque

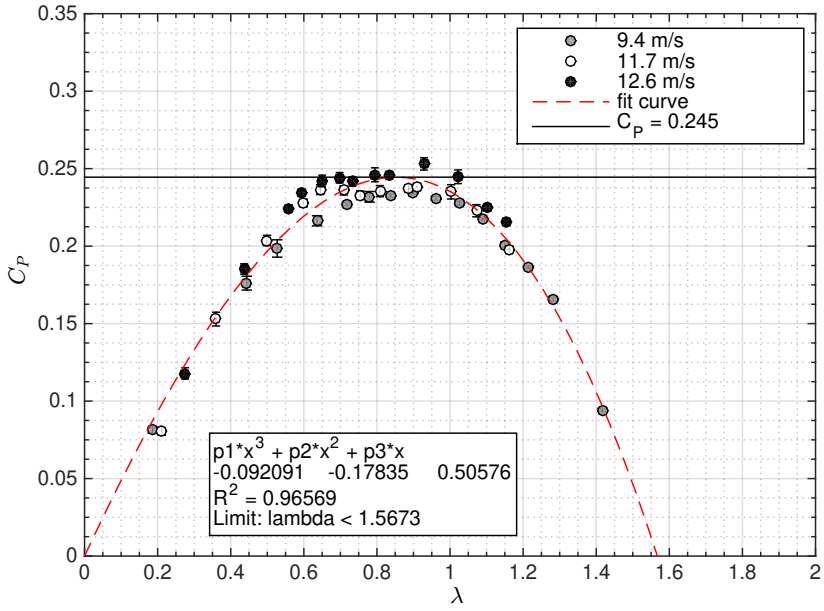

(c) Power Coefficient

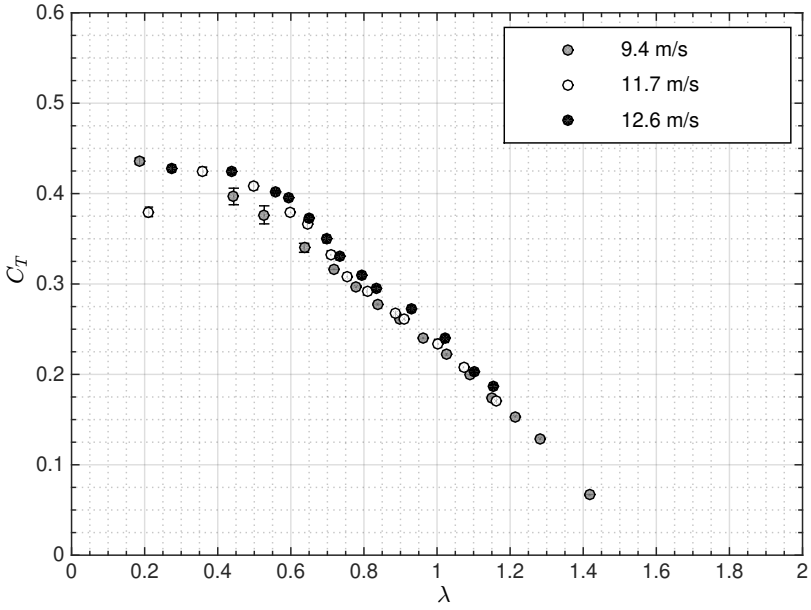

(d) Torque Coefficient

Fig. 7: Results obtained in the reference test (0deg_yE_nC_nD_nP)

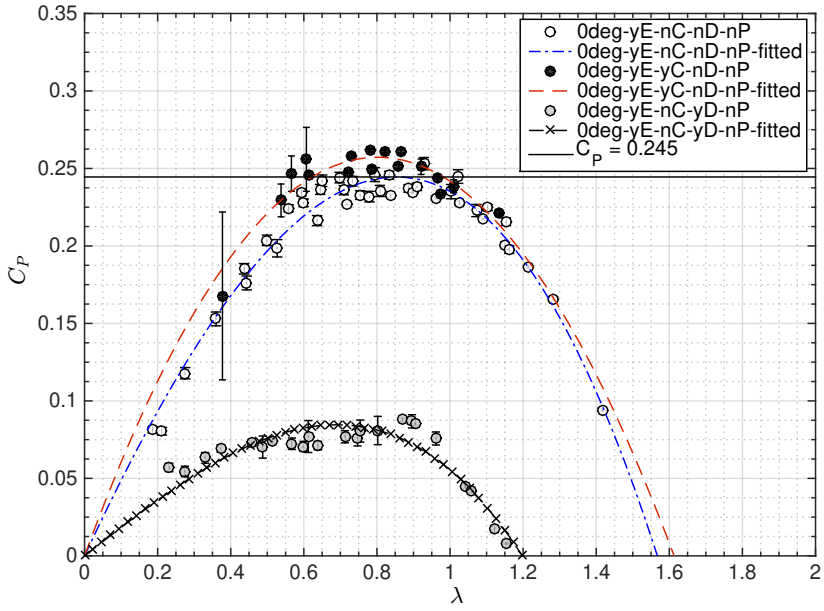

(a) Straight rotor without posts.

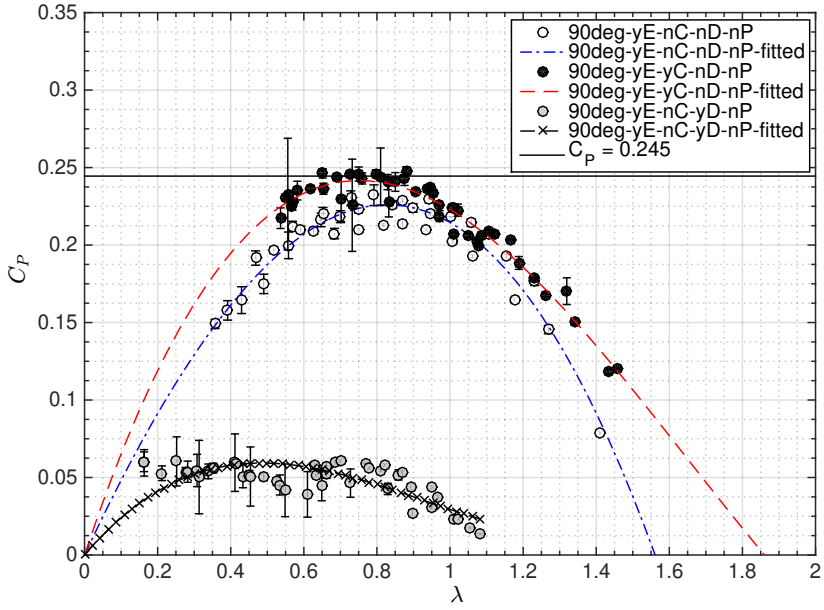

(b) Helical rotor with a step of 90°without posts.

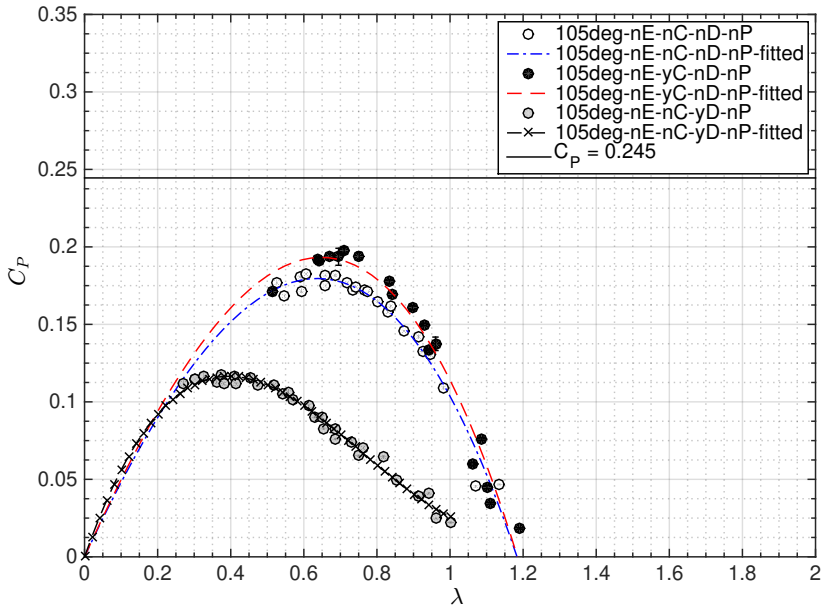

(c) Helical rotor with a step of 105°without posts and without end plates.

Fig. 8: Effect of the single appendages on the rotors' performance (white = without appendages, black = with Conveyor, gray = with Deflector).

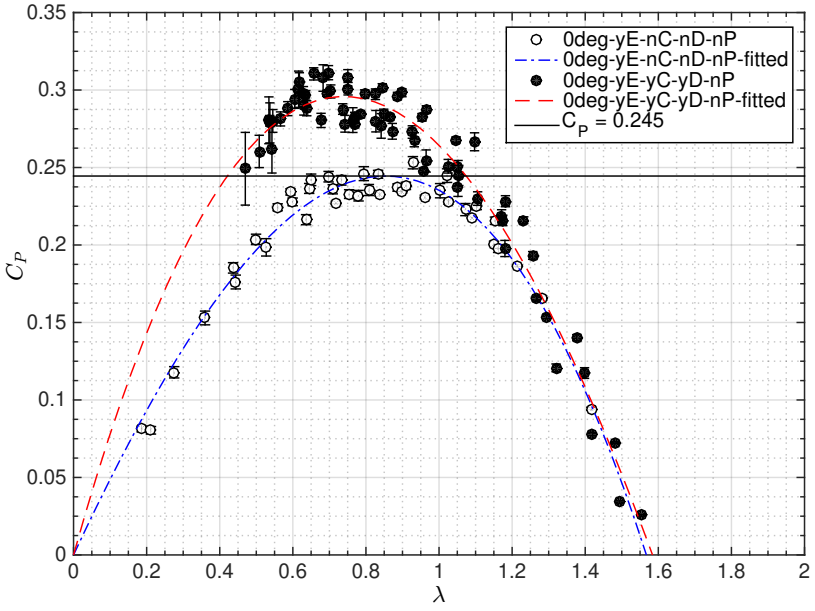

(a) Straight rotor without posts.

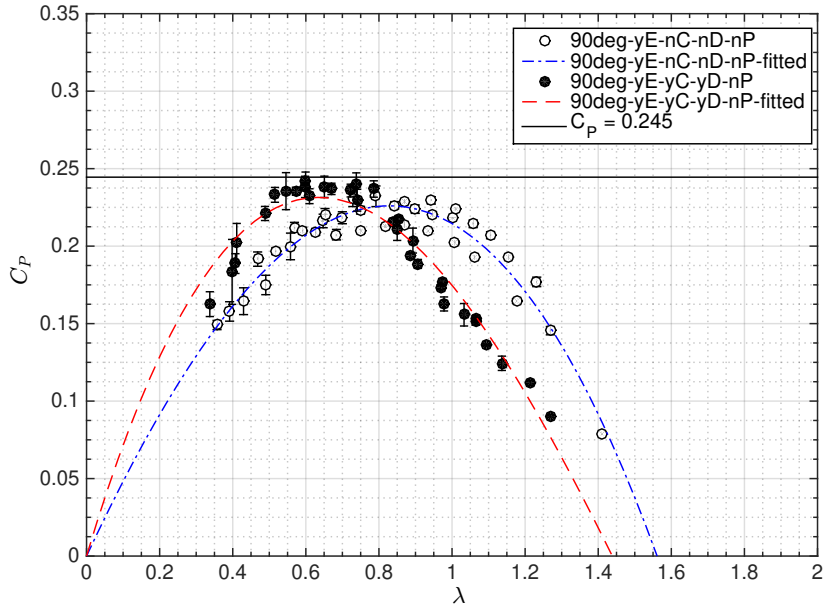

(b) Helical rotor with a step of 90°without posts.

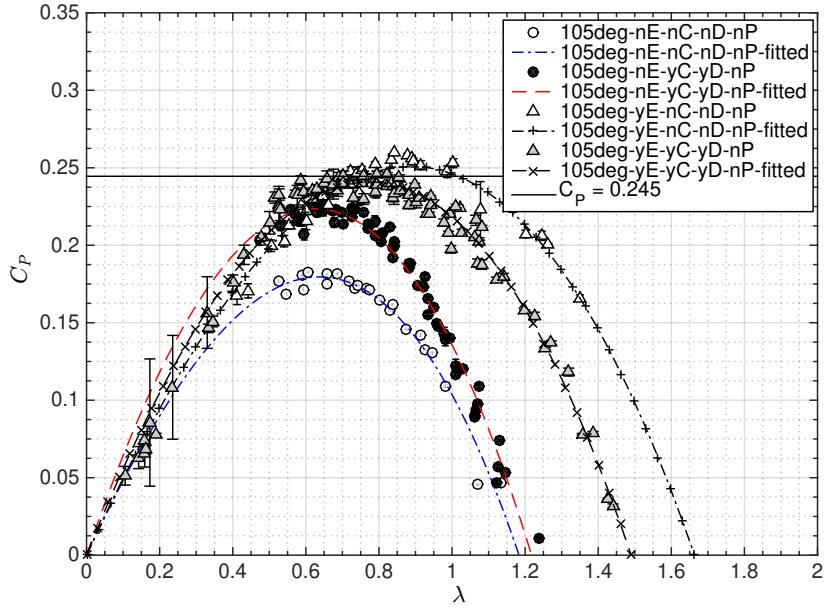

(c) Helical rotor with a step of 105°without posts and without end plates.

Fig. 9: Effect of the Conveyor + Deflector on the rotors' performance (white = without appendages, black/gray = with appendages).

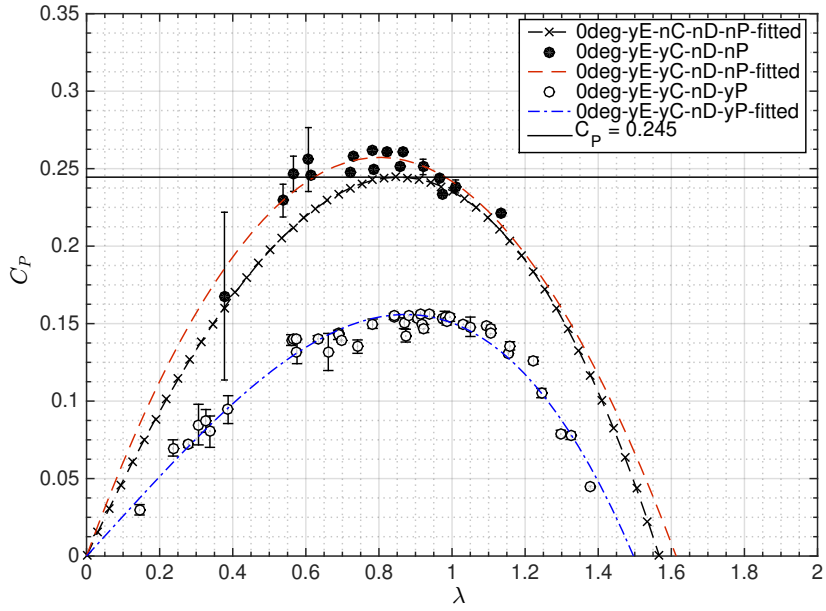

(a) Straight rotor.

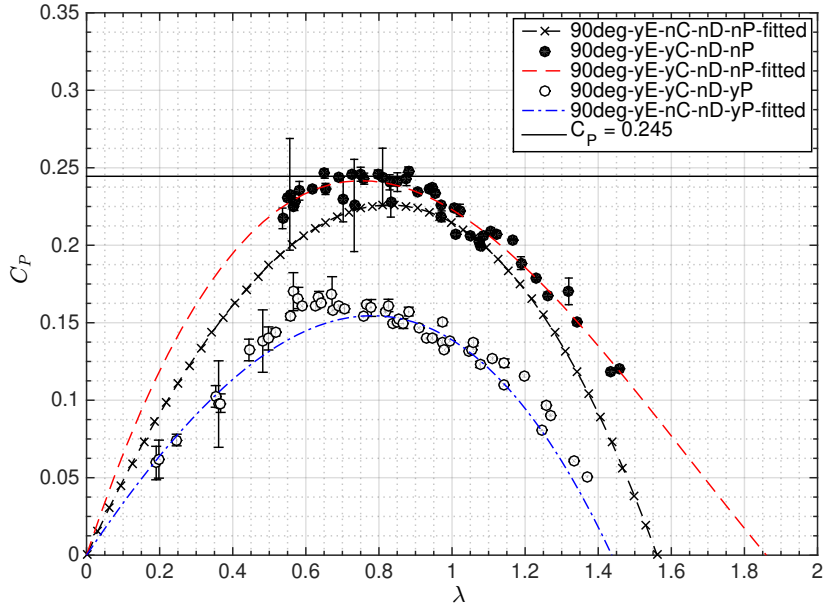

(b) Helical rotor with a step of 90°.

Fig. 10: Effect of the posts in the presence of the Conveyor.

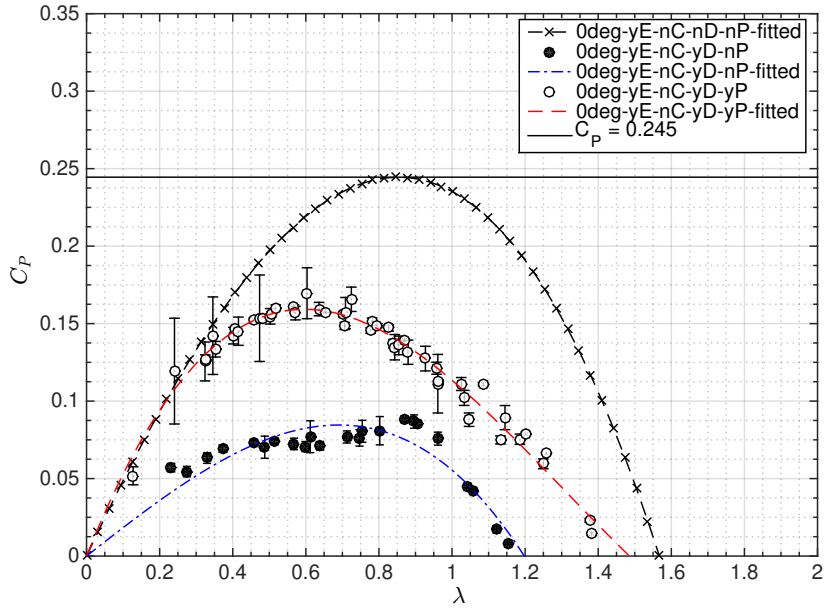

(a) Straight rotor.

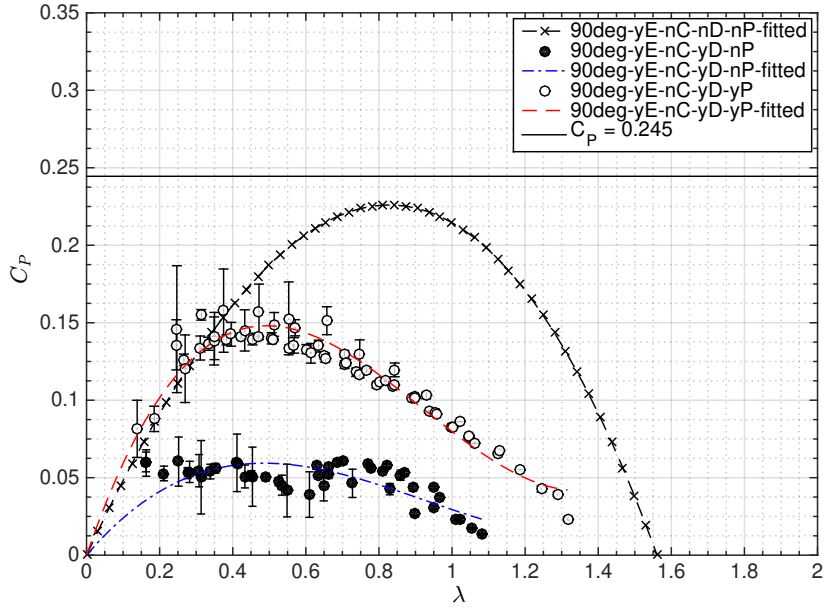

(b) Helical rotor with a step of 90°.

Fig. 11: Effect of the posts in the presence of the Deflector.

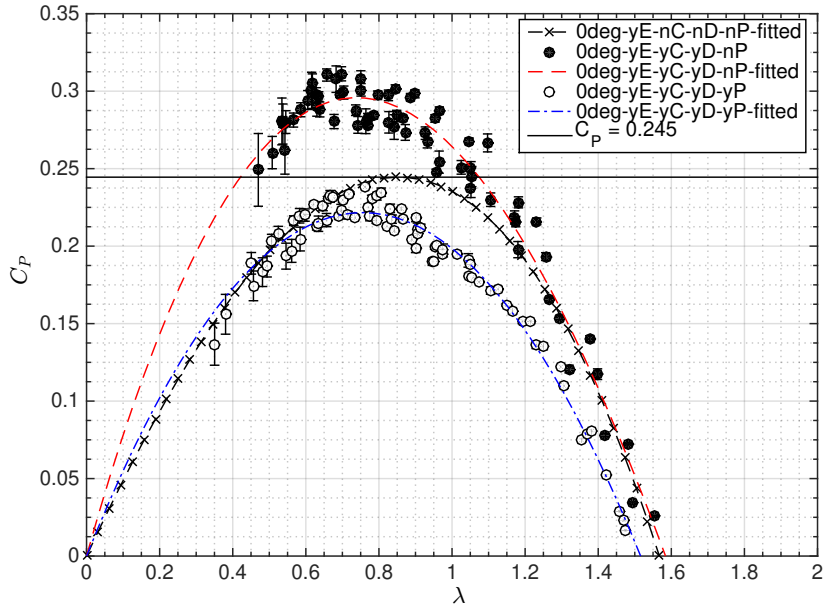

(a) Straight rotor.

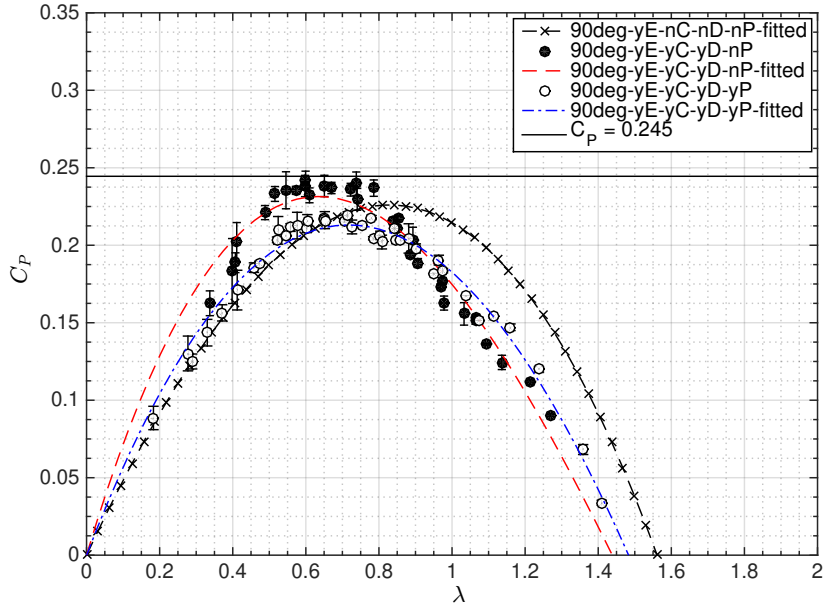

(b) Helical rotor with a step of 90°.

Fig. 12: Effect of the posts in the presence of the Conveyor and the Deflector.

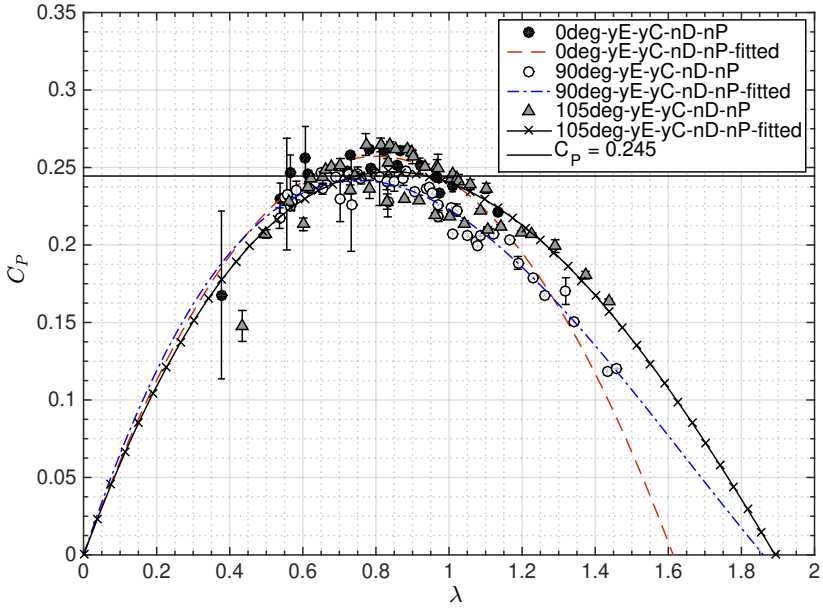

(a) Rotors with the Conveyor

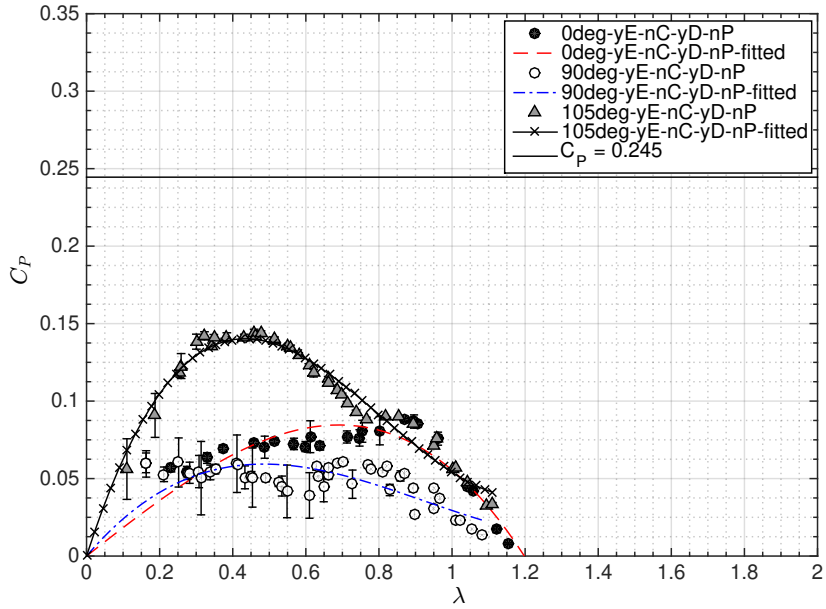

(b) Rotors with the Deflector

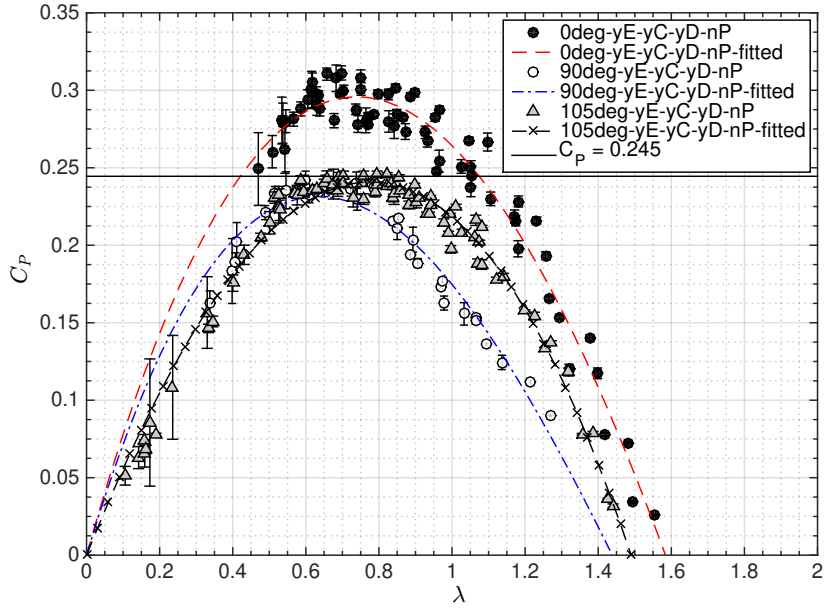

(c) Rotors with the Conveyor and the Deflector

Fig. 13: Effect of the twist in the presence of the external appendages.

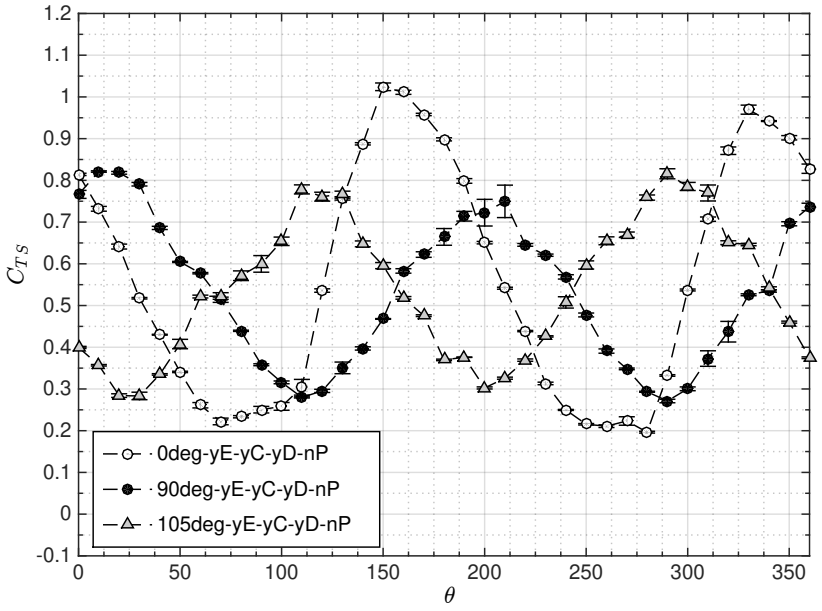

Fig. 14: Static torque for rotors with different helical step.

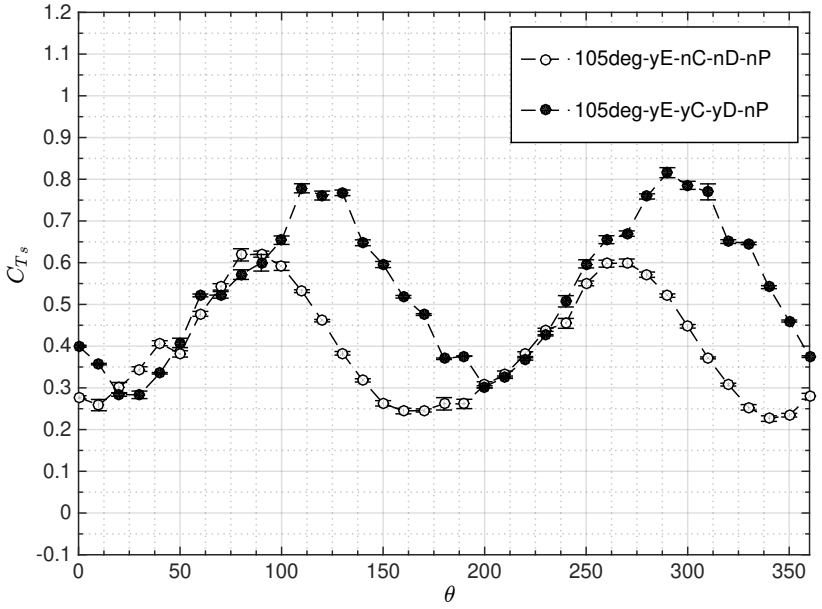

Fig. 15: Effect of external appendages on the angular distribution of the static torque.

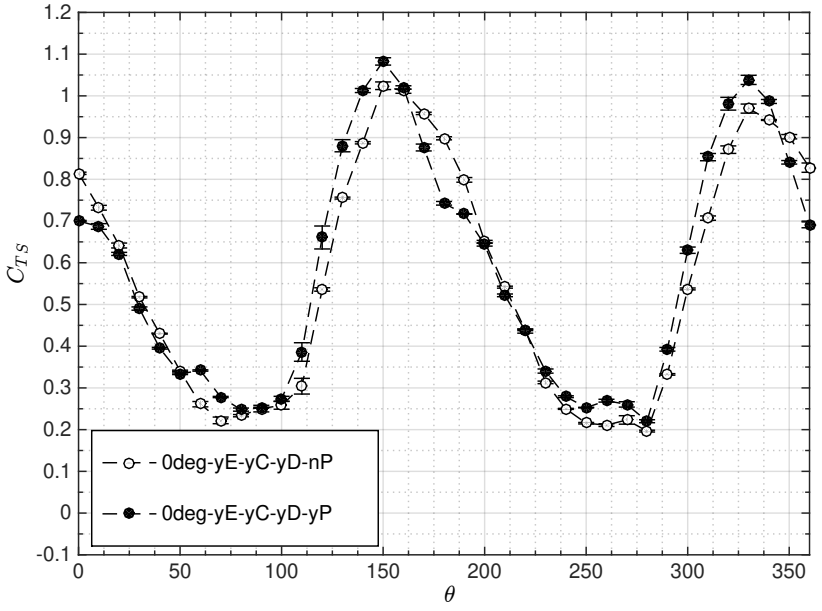

Fig. 16: Effect of posts on the angular distribution of the static torque.

Nomenclature

C_P	power coefficient	A_t	total frontal area (rotor and frame) $[m^2]$
C_T	torque coefficient	c	bucket chord $[m]$
C_{TS}	static torque coefficient	D	rotor diameter$[m]$
Re	Reynolds number	d	shaft diameter $[m]$
ϵ	blockage factor	D_{ep}	end plates diameter $[m]$
λ	tip speed ratio	l	lever arm length $[m]$
λ_c	tip speed ratio at $C_{P,max}$ occurs	P	power $[W]$
ν	air cinematic viscosity $[m^2/s]$	R	rotor radius $[m]$
ω	angular velocity $[rad/s]$	S	test section area $[m^2]$
ρ	air density $[kg/m^3]$	s	buckets spacing distance $[m]$
σ	standard deviation	T	torque $[Nm]$
θ	position angle $[^\circ]$	v	contract section velocity $[m/s]$
A	rotor swept area $[m^2]$		
a	buckets overlap distance $[m]$	v_∞	free stream velocity $[m/s]$

Optimal solution			
number of buckets	2	helical step	0°
overlap ratio (a/c)	10-15 %	shaft presence	no
spacing ratio (s/c)	0	number of stages	2
aspect ratio (A/D)	1-1.2	angle between stages	90°
bucket arc angle	180°	$C_{P,max}$ (1 stage)	$\simeq$0.24
end plates D_{ep}/D	1.1	$C_{P,max}$ (2 stages)	$\simeq$0.28

Table 1: Optimal configuration of a Savonius rotor with semi-circular blades.

Parameter	value
number of buckets	2
rotor diameter (D)	384 [mm]
shaft diameter (d)	37 [mm]
overlap ratio (a/c)	8.2 %
spacing ratio (s/c)	0
aspect ratio (H/D)	2.6
end plates (D_{ep}/D)	no - 1.1
bucket arc angle	180°
helical step	0°-90°-105°

Table 2: Geometric parameters of the rotors tested.

Helical step	$C_{P,max}$ without C	$C_{P,max}$ with C	Variation %
0	0.245	0.257	+4.9 %
90	0.226	0.242	+7.1 %
105*	0.18	0.193	+7.2 %

Table 3: Effect of the Conveyor on the $C_{P,max}$ of the rotors tested. (*) without end plates

Helical step	$C_{P,max}$ without D	$C_{P,max}$ with D	Variation %
0	0.245	0.085	-65.3 %
90	0.226	0.059	-73.9 %
105*	0.18	0.117	-35 %

Table 4: Effect of deflctor on $C_{P,max}$. (*) without end plates (D) deflector.

Helical step	$C_{P,max}$ no C+D	$C_{P,max}$ yes C+D	Variation %
0	0.245	0.296	+20.8 %
90	0.226	0.231	+2.2 %
105*	0.18	0.224	+24 %
105	0.251	0.241	-4 %

Table 5: Effect of appendages on $C_{P;max}$. (*) without end plates (C) conveyor (D) deflector.

Helical step [°/m]	Element	$C_{P,max}$ no P	$C_{P,max}$ yes P	Delta % $C_{P,max}$
0	C	0.257	0.156	-39 %
90	C	0.242	0.159	-34 %
0	D	0.085	0.159	+87 %
90	D	0.059	0.148	+151 %
0	C+D	0.296	0.222	-25 %
90	C+D	0.231	0.213	-7.8 %
105	C+D	0.241	0.209	-13.3 %

Table 6: Effect of posts and appendages on $C_{P,max}$. Rotors with End Plates. (C) conveyor (D) deflector (P) posts.

	0°	90°	105°
C	0.257	0.242	0.247
D	0.085	0.059	0.14
C+D	**0.296**	0.231	0.241

Table 7: Effect of the helical step and of the appendages on $C_{P,max}$. Rotors with end plates. (C) conveyor (D) deflector.

Test code	C_{TS}			ΔC_{TS}
	min	max	ave	
0deg_yE_yC_yD_nP	0.15	1.08	0.61	0.93
0deg_yE_yC_yD_yP	0.21	1.08	0.64	0.87
90deg_yE_yC_yD_nP	0.27	0.82	0.55	0.55
90deg_yE_yC_yD_yP	0.19	0.80	0.50	0.61
105deg_yE_nC_nD_nP	0.19	0.62	0.40	0.43
105deg_yE_yC_yD_nP	0.24	0.82	0.53	0.58

Table 8: Summary of the main results of the static tests

Test code	Helical step (°/m)	End Plates (E)	Conveyor (C)	Deflector (D)	Posts (P)	$C_{P,max}$	λ_c	λ_{max}	$2\sigma_{@max}$ ($\cdot 10^3$)
0deg_nE_nC_nD_nP	0	no	no	no	no	0.192	0.649	1.16	1.2
0deg_yE_nC_nD_nP*	0	yes	no	no	no	0.245	0.854	1.567	2.5
0deg_yE_yC_nD_nP	0	yes	yes	no	no	0.257	0.802	1.613	2.0
0deg_yE_nC_yD_nP	0	yes	no	yes	no	0.085	0.690	1.198	6.0
0deg_yE_yC_yD_nP	0	yes	yes	yes	no	**0.296**	0.739	1.584	4.1
0deg_yE_yC_nD_yP	0	yes	yes	no	yes	0.156	0.873	1.497	2.3
0deg_yE_nC_yD_yP	0	yes	no	yes	yes	0.159	0.597	1.485	4.4
0deg_yE_yC_yD_yP	0	yes	yes	yes	yes	0.222	0.755	1.516	2.0
90deg_yE_nC_nD_nP	90	yes	no	no	no	0.226	0.828	1.561	2.4
90deg_yE_yC_nD_nP	90	yes	yes	no	no	0.242	0.752	1.860	10.7
90deg_yE_nC_yD_nP	90	yes	no	yes	no	0.059	0.485	1.082	8.2
90deg_yE_yC_yD_nP	90	yes	yes	yes	no	0.231	0.634	1.439	5.6
90deg_yE_nC_nD_yP	90	yes	no	no	yes	0.155	0.781	1.437	nan
90deg_yE_yC_nD_yP	90	yes	yes	no	yes	0.159	0.760	1.495	2.1
90deg_yE_nC_yD_yP	90	yes	no	yes	yes	0.148	0.493	1.316	8.3
90deg_yE_yC_yD_yP	90	yes	yes	yes	yes	0.213	0.717	1.483	2.4
105deg_nE_nC_nD_nP	105	no	no	no	no	0.180	0.637	1.183	0.9
105deg_nE_yC_nD_nP	105	no	yes	no	no	0.193	0.648	1.185	1.6
105deg_nE_nC_yD_nP	105	no	no	yes	no	0.117	0.394	1.002	1.3
105deg_nE_yC_yD_nP	105	no	yes	yes	no	0.224	0.626	1.218	3.1
105deg_yE_nC_nD_nP	105	yes	no	no	no	0.251	0.889	1.664	2.7
105deg_yE_yC_nD_nP	105	yes	yes	no	no	0.247	0.824	1.89	3.2
105deg_yE_nC_yD_nP	105	yes	no	yes	no	0.14	0.434	1.3	2.3
105deg_yE_yC_yD_nP	105	yes	yes	yes	no	0.241	0.777	1.490	2.0
105deg_yE_yC_yD_yP	105	yes	yes	yes	yes	0.209	0.765	1.539	1.5

Table 9: Summary of the main results of the dynamic tests. (*) test taken as a reference.